New Mexico Geological Society

Downloaded from: https://nmgs.nmt.edu/publications/guidebooks/41



A mechanical model of keystone structures and reverse faulting for the southern Sangre de Cristo Mountains

R. J. Bridwell

1990, pp. 133-144. https://doi.org/10.56577/FFC-41.133

in:

Tectonic Development of the Southern Sangre de Cristo Mountains, New Mexico, Bauer, P. W.; Lucas, S. G.; Mawer, C. K.; McIntosh, W. C.; [eds.], New Mexico Geological Society 41st Annual Fall Field Conference Guidebook, 450 p. https://doi.org/10.56577/FFC-41

This is one of many related papers that were included in the 1990 NMGS Fall Field Conference Guidebook.

Annual NMGS Fall Field Conference Guidebooks

Every fall since 1950, the New Mexico Geological Society (NMGS) has held an annual Fall Field Conference that explores some region of New Mexico (or surrounding states). Always well attended, these conferences provide a guidebook to participants. Besides detailed road logs, the guidebooks contain many well written, edited, and peer-reviewed geoscience papers. These books have set the national standard for geologic guidebooks and are an essential geologic reference for anyone working in or around New Mexico.

Free Downloads

NMGS has decided to make peer-reviewed papers from our Fall Field Conference guidebooks available for free download. This is in keeping with our mission of promoting interest, research, and cooperation regarding geology in New Mexico. However, guidebook sales represent a significant proportion of our operating budget. Therefore, only *research papers* are available for download. *Road logs*, *mini-papers*, and other selected content are available only in print for recent guidebooks.

Copyright Information

Publications of the New Mexico Geological Society, printed and electronic, are protected by the copyright laws of the United States. No material from the NMGS website, or printed and electronic publications, may be reprinted or redistributed without NMGS permission. Contact us for permission to reprint portions of any of our publications.

One printed copy of any materials from the NMGS website or our print and electronic publications may be made for individual use without our permission. Teachers and students may make unlimited copies for educational use. Any other use of these materials requires explicit permission.

This page is intentionally left blank to maintain order of facing pages.

A MECHANICAL MODEL OF KEYSTONE STRUCTURES AND REVERSE FAULTING FOR THE SOUTHERN SANGRE DE CRISTO MOUNTAINS

R. J. BRIDWELL
GeoComp Inc., 3869 Montgomery NE, Albuquerque, New Mexico 87109

Abstract—In the southern Sangre de Cristo Mountains near Las Vegas, New Mexico, tilted basement controlled blocks are overlain by drape-folded sedimentary rocks which are cored by three reverse and imbricate thrust fault systems (Prucha et al., 1965; Baltz, 1972). The analytical stress solution for prediction of high-angle faults (Sanford, 1959) is extended to a finite element model containing an initial fault and subsequent failure history for a keystone structure. A keystone structure has a hanging wall, initially broken by a conjugate normal fault into an uplifted triangular butt and toe, and a footwall. A subsequent secondary conjugate normal fault dips into the antithetic fault in the triangular butt, more antithetic faults occur in the hanging wall, and imbricate thrusts occur at the triangular toe. Numerical stress orientations correlate with experimentally induced drape folds (Friedman et al., 1976). With field, experimental and numerical evidence corroborating an integrated keystone model, the concept of keystone structures is extended to genesis of the Rio Grande rift and Sangre de Cristo Mountains. Three tilted blocks are a sequence of high-angle reverse fault structures. Rift bounding faults may consist of the western antithetic conjugate normal fault and the eastern secondary normal fault. The uplifted triangular block forms the highlands of the Sangre de Cristo Mountains.

INTRODUCTION

The deformational history of the southern Sangre de Cristo Mountains is complex. During Laramide time (Late Cretaceous–early Tertiary), the Sangre de Cristo Mountains attained present structural outlines and moderate relief (Baltz, 1978), but during Late Eocene time the area was reduced to low relief (Baltz, 1978; Kelly and Duncan, 1984). Late Cenozoic regional uplift and normal faulting occurred in the Rio Grande rift during Miocene to Holocene time, followed by Pliocene and Quaternary volcanism (Woodward and Ingersoll, 1979). Geologic structures of the eastern flank of the Sangre de Cristo Mountains and the southern Raton basin of northern New Mexico consist of basement-controlled block faults and drape folds cored by high-angle reverse and imbricate thrust faults (Baltz and Bachman, 1956; Prucha et al., 1965; Baltz, 1972, 1978).

Field studies of reverse fault structures indicate brittle basement blocks have undergone uplift, tilting and faulting, creating drape folds cored by reverse faults in overlying ductile sedimentary rocks (Berg, 1962; Wise, 1963; Prucha et al., 1965; Baltz, 1972). Prucha et al. (1965) indicate the necessity of careful evaluation of the level of observation in interpreting surface geologic structures. For example, the characteristic profile of a reverse or upthrust fault consists of a vertical segment at the base, a high-angle reverse segment in the center and a low angle reverse segment at the earth's free surface. One may only see a portion of the entire structure, since erosional level generally limits observation. Each of these portions of a fault system provides different tectonic responses, e.g., compressional features are often observed in the low-angle portion of the structure, yet the entire structure is due to vertical uplift. Wise (1963), mapping gravity slides covering a low-angle portion of a reverse fault structure provided an excellent description of the formation of keystone grabens atop the hanging wall of reverse faults.

Analytical, experimental and numerical models provide insight for the deformation and stress history of reverse faults (Sanford, 1959; Friedman et al., 1976; this report). The initial analytical solution was an elastic analysis of vertical uplift on a continuous crustal basement block to predict the loci of a concave downward high-angle reverse fault and is included with an experimental model (Sanford, 1959). Experimental studies provided uplift of a brittle sandstone block containing a saw cut which produced high-angle reverse faults and a keystone graben in overlying ductile rocks of the hanging wall (Friedman et al., 1976). Stress trajectories were determined from orientations of microfractures and calcite twin lamellae. Successively younger reverse faults, thrusting upward, were shown to splay and thicken structures in the footwall while a graben formed atop the hanging wall. Reches and Johnson (1978) solved this problem analytically for compressible or incompressible, elastic or viscous multi-layers, providing analysis of monoclinal folds.

This numerical study provides two models of reverse faulting. The initial model contains a simple high-angle reverse fault and predicts that a single antithetic normal fault occurs in a triangular region of the hanging wall. The second model, containing the original reverse fault and new antithetic normal fault, consists of a hanging wall, a triangular region between antithetic normal and reverse faults and a footwall. Subsequent faults are predicted in the triangle; an initial normal fault conjugate to the antithetic normal fault in the butt of the triangle and later imbricate thrust faults in the compressed region in the toe of the triangle. Stress trajectories and reverse fault shapes in the initial numerical model are in good agreement with those of the experimental model of drape folds of Friedman et al. (1976). As uplift continues, a second antithetic normal fault is predicted in the uplifting hanging wall of the structure. The combined physical segments of the hanging wall, triangular region between the antithetic normal and reverse fault, and the footwall are named a *keystone structure* in this paper.

The keystone structural concept is applied to genesis of the southern Sangre de Cristo Mountains of New Mexico, for a comparison with structural observations of Prucha et al. (1965) and Baltz (1972). The structural section B-B′ of Baltz (1972) between Sapello and Elk Mountain of the Santa Fe Mountains contains a series of tilted basement controlled blocks with overlying drape-folded sedimentary rocks cored by three reverse and imbricate thrust fault systems. The reverse fault model of Sanford (1959) and models in this report are generalized to a basal uplift problem on a reverse fault. The simple single reverse fault model is then generalized to the multiple fault system of the southern Sangre de Cristo Mountains. The region between Elk Mountain and Sapello becomes the low-angle portion of the numerical reverse fault models containing imbricate thrust and reverse faults at the toe. The triangular segment of the keystone structure between the butt and toe becomes the uplifted region of the Sangre de Cristo Mountains between Mt. Baldy and Elk Mountain. The butt of the triangular segment, underlain by antithetic and conjugate normal faults, is analogous to the deep, bolson-filled fault grabens inferred from gravity studies of the San Luis, Española and Albuquerque basins bounding the Rio Grande rift.

GEOLOGIC HISTORY

The deformational history of the southern Sangre de Cristo Mountains is complex. During late Paleozoic time, a positive area, the San Luis uplift shed clastics into adjacent basins (Baltz, 1965). The Rowe-Mora

basin was east of the contemporaneous San Luis uplift. Mesozoic strata were deposited over the region followed by epeiorogenic uplift.

During Laramide time, the Sangre de Cristo Mountains emerged to attain present structural outlines. Late Cenozoic uplift of the entire region was contemporaneous with formation of the Rio Grande rift during Miocene to Holocene time, followed by Pliocene and Quaternary volcanism (Woodward and Ingersoll, 1979).

Geologic structures of the eastern flank of the Sangre de Cristo Mountains and the lower Raton basin of northern New Mexico include high-angle reverse and imbricate faults (Baltz and Bachrnan, 1956; Prucha et al., 1965; Baltz, 1972, 1978). Baltz and Bachrnan (1956) indicated most folding and complex faulting of Devonian through Lower Cretaceous rocks occurred in Laramide time and provided an interpretive cross section near Mora. Baltz (1972) provided a geologic cross section south of Sapello, containing folded Paleozoic rocks cored by imbricate thrust faults which steepen with depth. Figure 1 shows physiographic provinces associated with the Rio Grande rift and southern Sangre de Cristo Mountains of northern New Mexico. The position of section A-A′ is the approximate loci of two geologic sections from Baltz and Bachman (1956) and Baltz (1972) and the keystone structural interpretation of this paper.

STRUCTURAL ANALYSIS OF GEOLOGIC STRUCTURES

Evaluation of the structural origin of the southern Sangre de Cristo Mountains can benefit from prior studies of similar basement controlled structures on reverse faults which were concave downward or steepen with depth. Examples include the Wind River Mountains (Berg, 1962), Owl Creek Mountains (Wise, 1963), Big Horn Mountains and Laramie Range (Prucha et al., 1965), and Sangre de Cristo Mountains (Prucha et al., 1965; Grose, 1972; Tweto, 1975) and Front Range (Berg, 1962) of the Wyoming province of the Rock Mountain foreland. Baltz and Bachman (1956) originally considered the southern Sangre de Cristo Mountains to be controlled by imbricate thrusts which shallow with depth. Wise (1963) defined the Owl Creek Mountains to result from basement block faulting of reverse or upthrust faults where Paleozoic rocks drape over the forcing basement block. Prucha et al. (1965) defined numerous ranges—including the southern Sangre de Cristo Mountains—to be the result of basement block upthrusts. Baltz (1972) defined the same basement faults from Baltz and Bachrnan (1956) as steepening with depth. These interpretations of faulted blocks which are cut by reverse faults steepening with depth are consistent with reverse fault models of this report.

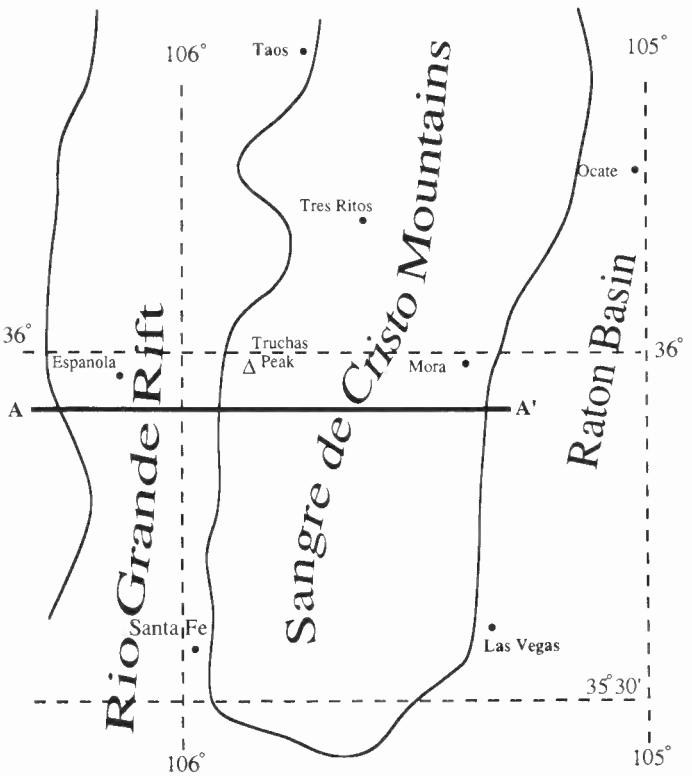


FIGURE 1. Physiographic provinces of the southern Sangre de Cristo Mountains of northern New Mexico. Section A-A′ is the approximate loci of the interpretive geologic cross section of Baltz and Bachman (1956) and the structural cross section from Baltz (1972, section B-B′) and the keystone structure of mechanical model from this report.

The Owl Creek Mountains consist of basement blocks exposed at higher elevations bounded by normal and reverse faults across 8 km of relief on the Wind River basin (Wise, 1963). Wise interpreted the frontal structure of the Owl Creeks as a concave downward high-angle reverse basement fault which splays and becomes low angle near the surface. A keystone graben is formed on the upthrown basement block where normal faulting occurs. Subsequent gravity sliding from the front of the upthrown block complicates the structural interpretation.

Basement controlled deformation of the southeastern Sangre de Cristo region near Mora was structurally analyzed by Prucha et al. (1965). Deformation is characterized by differential vertical uplift of discrete north-south-striking granitic blocks, bounded on the east and west sides by high-angle reverse faults. Upthrown sides produce a step-like arrangement of tilted igneous and/or sedimentary blocks dipping 10° westward and ascending to the west. Downthrown blocks show steeply dipping sedimentary units whose attitude ranges from sub-horizontal through vertical to overturned. The average dip is moderate to steep. Overlying sedimentary rocks have been draped as monoclines over the blocks to form asymmetrical anticlines on the upthrown west side of blocks and asymmetrical synclines on the downthrown eastern side. Asymmetrical folds are clearly related to reverse faults. Sedimentary rocks capping basement blocks are not deformed away from the margins of the blocks except for the westward tilting in unity with the underlying basement (Prucha et al., 1965).

Prucha et al. (1965) analyzed numerous ranges in the Wyoming province east of the Colorado Plateau from Montana to New Mexico to define a distinctive structural style. The dominant structural style for basement deformation is block faulting separating basins containing 2.5–5 km of sedimentary rocks. Individual basement blocks are bounded by upthrust faults which commonly die out upward into monoclinal flexures in overlying sedimentary rocks. Tilting of basement blocks produces a characteristic asymmetry of individual uplifts and basins. Originally horizontal, yet relatively ductile, sedimentary beds change attitude through tilting, up-dip extension of basement faults and buckling in local zones of horizontal compression related to upthrust or reverse faulting.

Baltz (1972, section B-B′) provides a similar structural interpretation near Sapello. Major topographic and structural highs of El Cielo Mountain, an extension south of Hermit Peak, and the Creston are folded and cored by faults. Younger Paleozoic rocks are exposed in the lower plates as one progresses eastward whereas Precambrian rocks core western reaches. Imbricate faults, splaying upward, are more numerous and generally involve sedimentary rocks. At depth, these faults are concave downward, reversing prior work of Baltz and Bachman (1956). Faults were projected to depths of 2 (Baltz, 1972) and 4 (Baltz and Bachrnan, 1956) km. Geologic structure sections of the southeastern Sangre de Cristo Mountains are shown in Figure 2. Two major types of rocks are shown in these interpretations: undifferentiated ductile Paleozoic carbonates and brittle Precambrian metavolcanic and granitic igneous rocks.

HISTORY OF ANALYTIC AND NUMERICAL MODELING

In the last 40 years, primary mathematical techniques have developed from analytic elastic and viscous solutions to advanced finite element techniques for creep and large deformation. Sanford (1959) provided a stress solution of two biharmoic equations to an elastic problem of crustal uplift. Assuming a rectangular elastic structure 5 km deep, a simple step function was applied across the base to simulate vertical uplift, body forces were imposed, and lateral loads confined horizontal motion. This solution predicted the loci of a high-angle reverse fault.

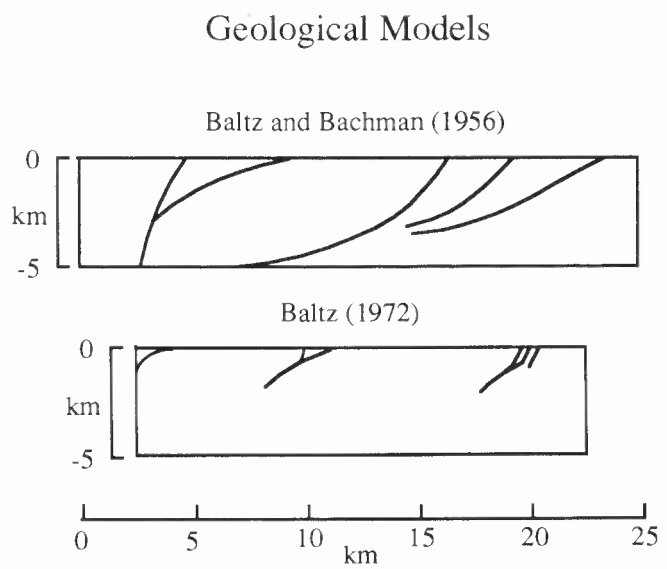


FIGURE 2. Geological structure sections from Baltz and Bachman (1956) and Baltz (1972). Each section has been compiled for this report at a 1:1 scale in kilometers and reflects published information.

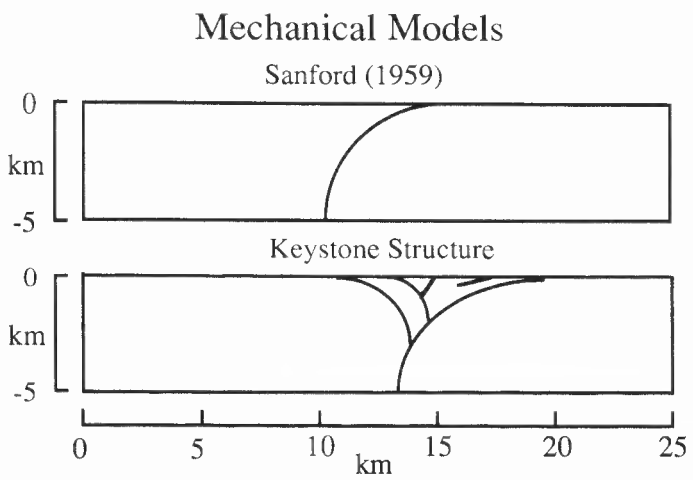


FIGURE 3. Mechanical models of reverse faults include analytical model of Sanford (1959) and the resulting faults predicted by numerical models of this report. The initial high-angle reverse fault zone loci from Sanford (1959) is shown in the upper figure. An antithetic normal fault is predicted in the hanging wall. Subsequent models containing the reverse and antithetic faults, shown in the lower figure. This fault system forms a triangle, predicts normal faults conjugate to the antithetic fault at the butt of the triangle, imbricate thrust faults at the toe of the triangle, and a second antithetic normal fault. The entire model is called a keystone structure model.

Subsequent works on viscous solutions of monoclinal folds have been provided by Johnson and Honea (1975) and Reches and Johnson (1978).

Advances in finite element techniques through varied geometrical assumptions, inclusion of several physical phenomena such as creep, heat transfer, Darcy flow, and faulting, as well as coupling of these terms, have provided powerful modeling capabilities (Anderson, 1986). Sangre is an elastic, viscous, finite-element code which has been applied to modeling large motions on thrust plates, hydrocarbon migration, far field analysis of nuclear waste repository sites, thermal stress cracking in ice fields, and continental rift tectonics (Bridwell, 1990).

We provide a series of time dependent finite element models to extend previous analytical solutions of Sanford (1959). The first model includes a primary high-angle reverse fault and predicts an antithetic normal fault which dips toward the high-angle reverse fault, joining at depth and suggesting formation of a *keystone structure*. A second structural model initially includes one reverse and one antithetic fault. The *keystone structure* consists of a hanging wall, a triangular butt and toe, and a footwall. Simulations indicate the triangle is subsequently broken by normal faults conjugate to the antithetic normal fault at the butt as well as imbricate thrust faults in the toe. A second antithetic normal fault occurs in the buttress formed below the keystone in the hanging wall of the reverse fault. Stress is reduced in the footwall, which does not fault. The analytical and numerical models are shown in Figure 3 as mechanical models of reverse faulting.

STRUCTURAL ANALYSIS OF GEOLOGICAL AND MECHANICAL STRUCTURES

Brittle, high-strength Precambrian granitic rocks fracture easily as opposed to Paleozoic carbonate rocks which are ductile and flow (Handin et al., 1963). Igneous rocks, mechanically stronger than the sediments, act as a ram or buttress to force brittle block deformation during long term uplift. Sedimentary rocks act as a passive layer, reacting ductility or folding in response to imposed forces. In structural interpretations of this report, we demonstrate only the dominant behavior of the stronger, brittle granitic crust, including the faulting processes it incurs. This behavior is assumed to cause more passive folds and associated faulting which occur in ductile sedimentary rocks.

In the elastic analysis of Sanford (1959) and the numerical analysis of this report, materials are treated as brittle igneous rocks, and sediments are ignored. Sanford (1959) predicted the loci of a high-angle reverse fault. In this report, the Mohr-Coulomb brittle shear failure criterion is used in conjunction with occurrence and orientation of tensile stresses to predict failure. This model predicts two varied states of stress: normal faults based on occurrence of extensile states of stress in the hanging wall near the free surface where the shear direction is subsequently activated and imbricate thrust faults from Mohr-Coulomb analysis for shear behavior in the wedge edge of the hanging wall.

By modeling and interpreting features of the strong igneous basement, a series of models evaluates the interactions of dynamically changing stress fields associated with numerous faults in brittle basement rocks. Initially, a *keystone structure* is formed with subsequent genesis of normal faults at the buttress of the keystone and imbricate thrust faults in the toe. Attendant brittle failure includes a second antithetic normal fault as uplift continues.

FINITE ELEMENT MODELS OF REVERSE FAULTS

Dynamic finite element models provide mechanical analyses of complex, faulted geologic structures. These analyses consist of numerical solutions to boundary-value problems with mixed boundary conditions imposed on both continuum bodies and along discrete slide lines or faults. In geologic terms, two rock masses are separated by a high-angle reverse fault. The hanging wall is uplifted and deformed as it moves past the footwall. There is no friction along on the fault.

Reverse fault model

Boundary conditions consist of a free surface, where the normal and shear stress are zero, a lateral compression from horizontal surface tractions, body forces which occur throughout the structure, and a constant velocity step function imposed on the base of a continuum model containing a reverse fault. Slide line (or fault) elements (Anderson, 1986) are placed along the predicted trajectory of a high-angle reverse fault (Sanford, 1959) within the model. The hanging wall is pushed up along the fault whereas the footwall is fixed in space. Internal stress states are calculated based on penetration or separation of nodes along the fault and combinations of imposed stresses. The initial structural geometry for the reverse fault model is shown in Figure 4.

Keystone structure model

Boundary conditions, surface tractions and body forces are imposed in a fashion similar to conditions for the reverse fault model. The major difference concerns the occurrence of a second normal fault predicted by the previous model. Slide line (or fault) elements are placed along the trajectory of a high-angle reverse fault and the trajectory of a *new*

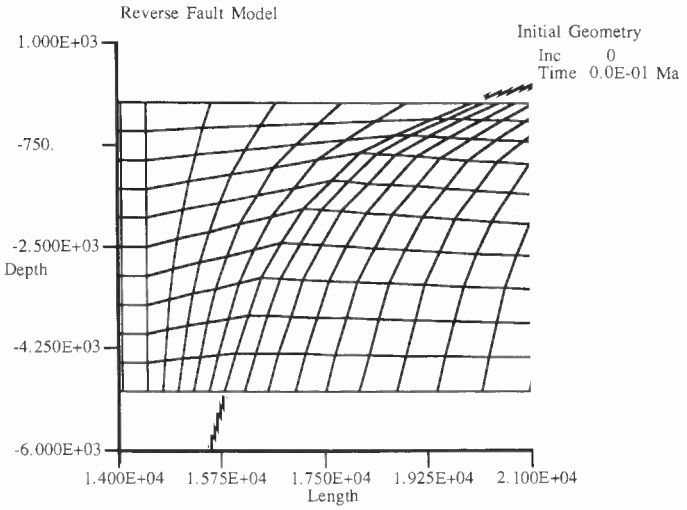


FIGURE 4. Initial finite element mesh for a reverse fault model. The lines extending from the upper and lower boundaries of the mesh show the position of the reverse fault.

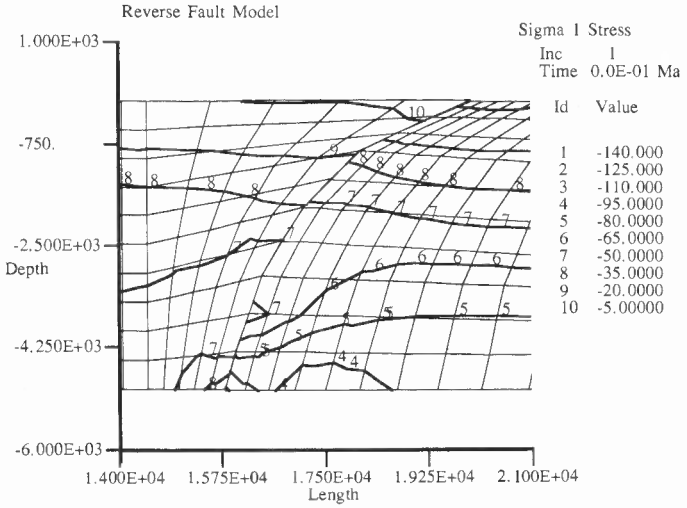


FIGURE 6. Contours for the initial state of Maximum Principal Compressive Stress s_1 for the reverse fault model prior to uplift. This engineering stress generally acts on horizontal planes in the model except in the region of the reverse fault zone. This plot shows a decrease in stress magnitudes as depth increases along the fault. Stress contours are discontinuous across the fault. Stress magnitude is decreased in the hanging wall above the reverse fault as the hanging wall unloads. As noted from engineering sign convention, negative stress is compressive whereas positive stress is tensile. Stress contours in MPa.

antithetic normal fault predicted by the reverse fault model. The initial structural geometry for the keystone structure model is shown in Figure 5.

DEFORMATION AND STRESS ANALYSIS

In geological conventions, compressive stress is positive and tensile stress is negative. The engineering stress sign convention, compression is negative and tension is positive, is used for Sangre and throughout this paper (see Appendix for discussion). The engineering Maximum Principal Compressive Stress as equivalent to the geologic Minimum Principal Compressive Stress. This paper interprets the engineering maximum principal compressive stress, σ_1, as the smallest absolute value of the stress. Normals to σ_1 act in the horizontal plane, except in perturbed regions near the fault zone(s). The geologist will recognize that in their terminology, this stress is a minimum principal compressive stress.

Reverse fault model

The least compressive principal stress, σ_1, is dominantly horizontal external to the fault zone, as shown as Figure 6. There is a smooth variation of stress in the model, except near the fault zone. At depths greater than -1 km, stress contours are offset across the reverse fault, showing a decrease of stress in the hanging wall where the reverse fault begins to attain shallower dips. As motion increases, magnitudes of these stresses change. There is an increase of stress in the hanging wall near the base, but there is a general decrease of stress in the fault zone because the hanging wall is unloading the footwall. For example, a point to the right of the fault at a depth of about -2.5 km has decreased horizontal stresses by about 15 MPa.

Although stress is initially compressive, uplift creates some extension. At the surface, stresses in the hanging wall become positive or tensile for σ_1, reaching average depths of about -700 m. A zone of tensile stress reaches down to the fault zone at depths of -1.5 km in the footwall beneath the reverse fault. Compressive stresses are diminished by a factor of 2 below this zone due to uplift.

The minimum principal compressive stress σ_3 is vertical in the model, and for a Poisson's ratio of 0.25, is about 3 times σ_1. For lithostatic conditions, $\sigma_1 = (n/(1-n))\sigma_3$. In geologic terms, σ_1, the vertical maximum principal compressive stress, is about 3 times σ_3 (see Appendix and Figure 18 for clarification).

The weight of the relatively unsupported hanging wall, which acts like a cantilever, combined with tension, causes the hanging wall to fail. The Mohr-Coulomb failure criterion indicates a new antithetic normal fault occurs in the hanging wall to form a keystone triangle. The predicted geometry of the concave downward antithetic normal fault is shown in Figure 7. The sense of concavity is opposite that of the original reverse fault.

The stress orientations of the maximum principal compressive stress during uplift are shown in Figure 8 when uplift has progressed for 0.042 Ma. The maximum principal compressive stress σ_1 is horizontal away from the reverse fault (controlled by assumed uniform horizontal displacements), but is curved concave downward in the hanging wall (controlled by the fault orientation) within several km of the reverse fault as uplift occurs. These are essentially the horizontal stresses in the model due to body forces and opposing uplift, except in the immediate vicinity of the fault where fault interaction modifies the stress field. In the footwall, this stress is nearly horizontal near the base of the model, curving concave upward beneath the region where the reverse fault changes from high to low angle. These orientations only change a few degrees during the next 0.042 Ma of deformation.

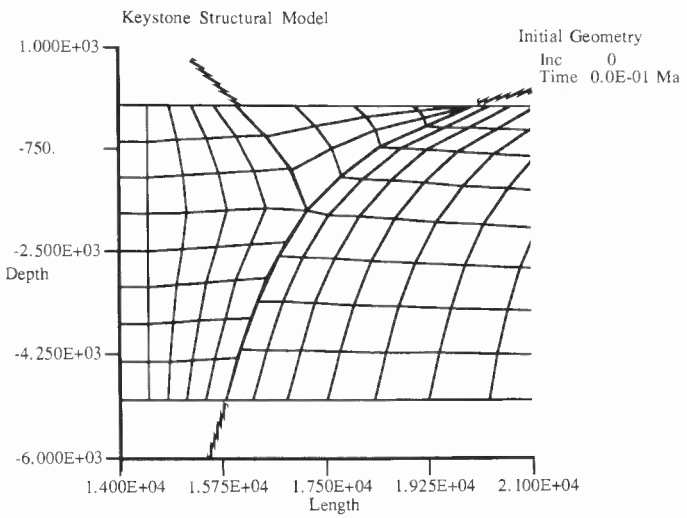


FIGURE 5. Initial finite element mesh for a keystone structural model. The lines extending from the upper and lower boundaries of the mesh show the position of the reverse and antithetic normal faults.

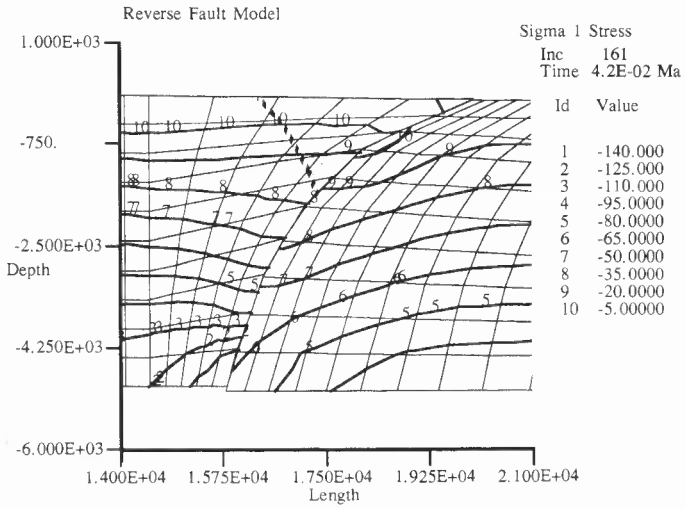


FIGURE 7. Maximum Principal Compressive Stress s_1 of reverse fault model at 0.042 Ma. As uplift progresses, compressive stress increases at the base of the hanging wall whereas tensile stress begins to work downward from the surface. The footwall begins to unload as stresses decrease, noticeably changing the stress effects in the region of the reverse fault. An antithetic normal fault (shown by the hachured line) is predicted to occur in the hanging wall from the surface to the reverse fault.

Keystone model

Variations of σ_1 for the keystone model is shown as Figure 9. There is a smooth variation of stress in the model, except near the fault zone. Introduction of the keystone graben causes varied stress concentrations near the base of the triangle. Tensile stress reaches deeper into the keystone. Compression is enhanced where the triangle is being uplifted by the hanging wall and rotating into the footwall at its base. At depths greater than -1 km, stress contours have been offset across the reverse fault, showing a decrease of stress in the hanging wall where the reverse fault begins to attain a shallower dip.

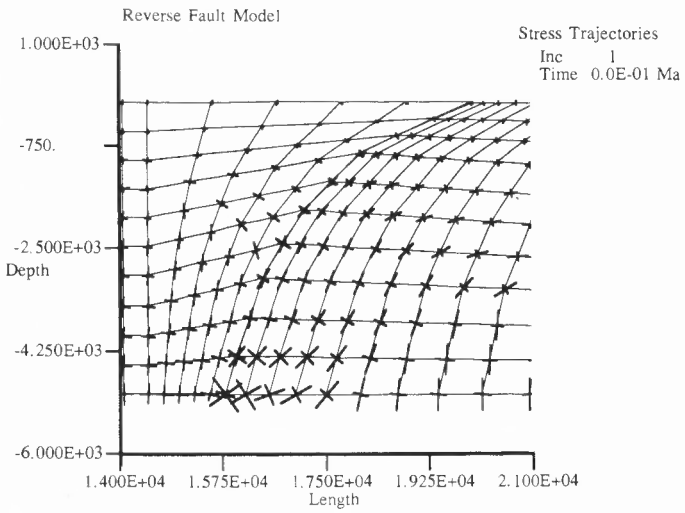


FIGURE 8. Stress trajectories for initial stresses of reverse fault model. Solid lines represent compressive stresses. The principal compressive stress is horizontal away from the reverse fault (controlled by assumed uniform horizontal displacements), but is curved concave downward in the hanging wall (controlled by the fault orientation) within several km of the reverse fault as uplift occurs. These stress trajectories represent the absolute values of the maximum principal stresses as shown in engineering notation where compression is negative and tension is positive. These stresses appear to be rotated 90° to experimental values (see Appendix).

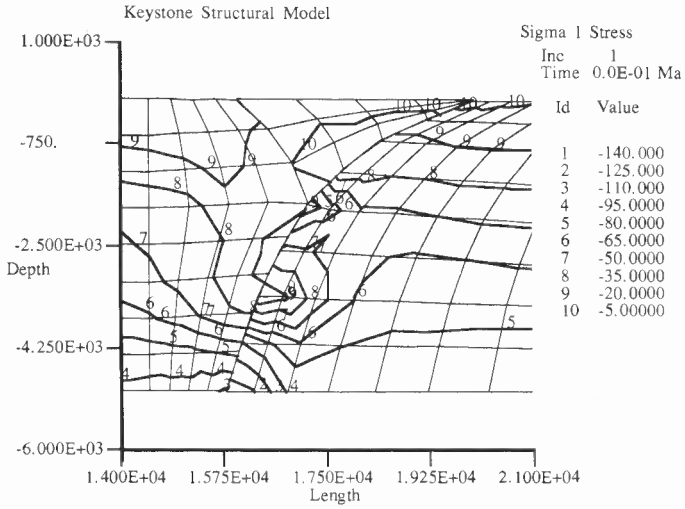


FIGURE 9. Change of initial stress magnitudes when a second antithetic normal fault is introduced in the keystone model. Stress concentrations occur at the base of the model and extensile stress reaches deeper into the keystone triangle. Stress contours are offset across the fault as the footwall is unloaded.

As motion increases, magnitudes of these stresses change from extensile to compressive as shown in Figure 10. The initial decrease of stress in the triangle reverses with further uplift. There is a general increase of compressive stress in the triangle as the hanging wall is uplifted.

STRESS AND FAILURE ANALYSIS IN KEYSTONE TRIANGLE

Stress magnitudes change within the triangular region in the early history of keystone motion, as shown in Figure 11. Tensile stresses are shown by the stippled region. Tension occurs from the top of the normal fault out and down -1 km into the triangle. A second zone of tensile stress occurs at the surface 1.5 km behind the tip of the low-angle reverse fault and extends downward to the reverse fault at depths of -1.2 km. The larger tensile region near the toe has increased size and magnitude. Compressive principal stresses occur in two areas from the surface to where keystone triangle, hanging wall, and footwall meet. The other occurs at the toe of the hanging wall above the low-angle

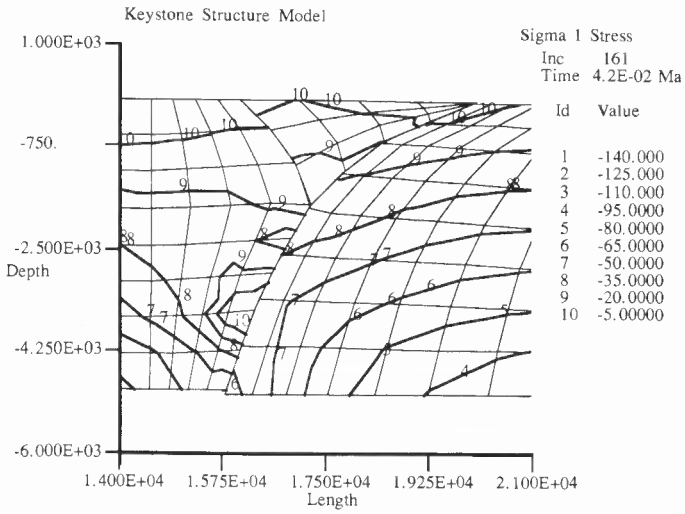


FIGURE 10. Stress magnitudes at an intermediate stage in uplift of the hanging wall for the keystone model at 0.042 Ma. The initial tensile stress in the butt of the triangle has become compressive as compressive stresses have increased in the triangular keystone. Compression in the toe of the triangular keystone presages formation of imbricate thrust faults.

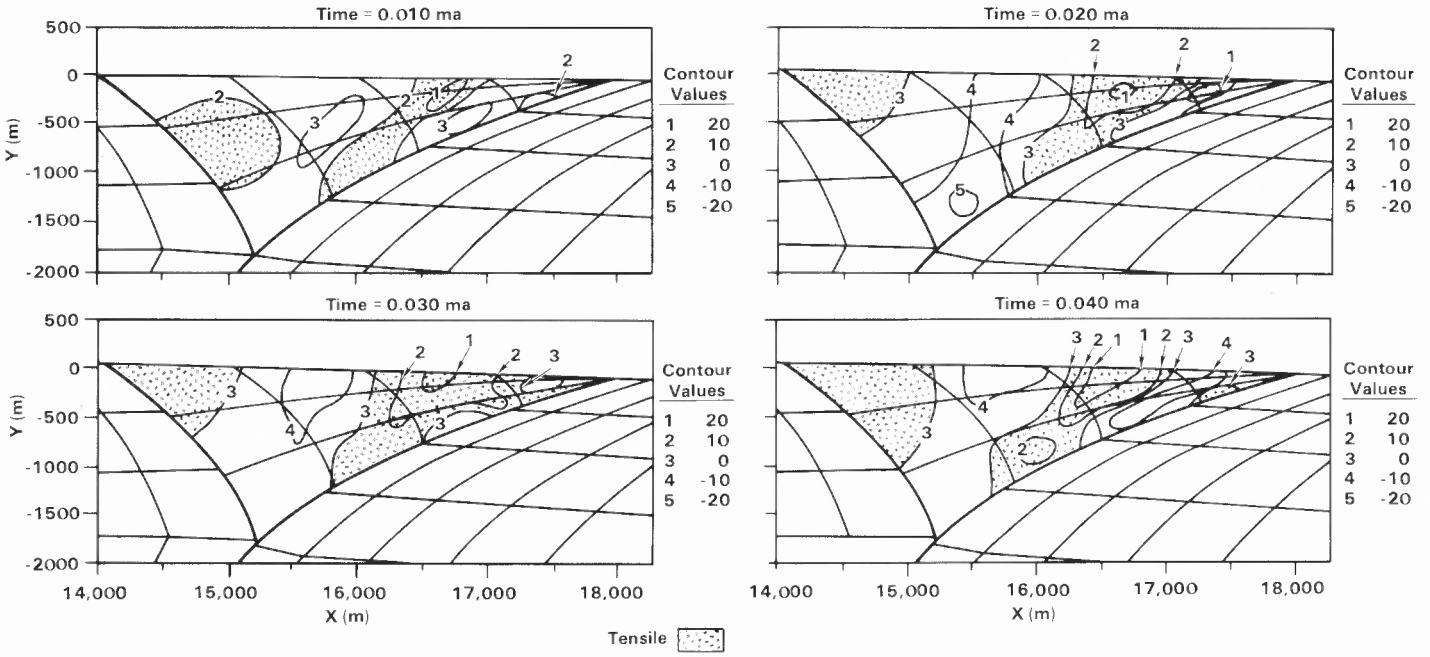


FIGURE 11. Keystone triangular region showing enhanced stress contours during 0.04 Ma of deformation. Zones of tension occur at the butt and near the toe. Compression occurs above the base of the triangular keystone and in the toe.

reverse fault and dips back more steeply than the low-angle reverse fault.

From the position of two tensile stress regions, a series of secondary graben structures can occur in the original keystone triangle model. The smaller secondary graben occurs conjugate to the new antithetic normal fault at the butt of the triangle and extends to depths of about −0.5 km. The larger secondary half-graben occurs where a normal fault extends from the surface to the high-angle reverse fault at depths of −1.2 km near the compressive toe of the keystone triangle.

Stress orientations and failure patterns which occur in the triangular portion of the keystone structure show time dependent variations. There is some initial variation in stress orientation, with the maximum principal (or tensile) stresses occurring in the middle of the triangle at the toe about 40° to the low-angle reverse fault, then rotating subparallel to the low-angle reverse fault. With continued uplfit, two regions of tensile and compressive stresses occur in the keystone triangle as shown in Figure 12.

Coulomb shear failure occurs in the toe of the keystone triangle near

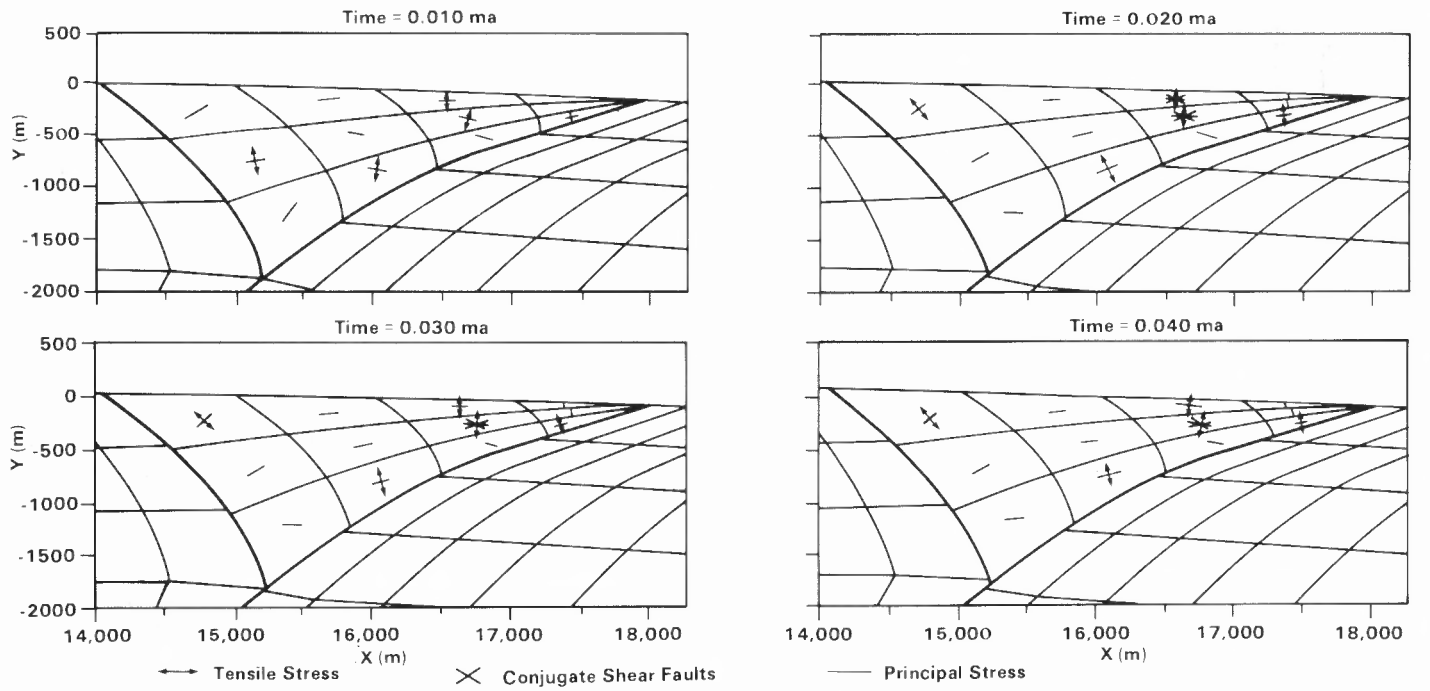


FIGURE 12. Stress trajectories in the triangular keystone region. This combination of stresses indicates a set of normal faults could occur at the butt of the triangle. Extension fractures and potential faults whose attitude is subparallel to the surface are shown by outward arrows, where principal stress is tensile. Mohr-Coulomb shear and extension fractures are shown by three lines and an arrow normal to the center of these lines. Imbricate thrust faults would occur in the regions where Mohr-Coulomb was calcualted, e.g., the region from the toe back a distance of 2 km into the keystone triangle. This region would undergo a complex sequence of normal and thrust faults with continued deformation.

the surface. Shear faults either dip steeply toward the low-angle reverse fault at the toe or are subparallel to the low-angle portion of the reverse fault. Low-angle conjugate shears would have secondary significance subparallel to the reverse fault. A set of conjugate normal faults would develop where the maximum principal compressive stress has rolled over and become normal to the low-angle reverse fault.

The relative motion of two points on the keystone triangle block at the butt of the triangle near the normal fault and toe of the low-angle portion of the reverse fault consists of counterclockwise rotation down the normal fault through dip slip motion and upthrust along the low-angle portion of the reverse fault through thrust motion. The footwall of the normal fault has undergone some shear response, as noted by nodal penetration of the uplifting hanging wall into the down dropped secondary graben at the butt of the triangular block. The base of the keystone triangle moves into a void created at the triple point forming the intersection of the hanging wall, footwall, and triangular block. Although there is initial uplift along the new normal fault, this motion quickly becomes dip slip and is of secondary magnitude compared to lateral motion of the keystone. We have shown that thrust motion is the dominant motion on the large keystone triangle near the toe. Thrust faults in the toe could become numerous and splay into imbricate thrust structures.

The continued displacement history beyond the limited uplift of the numerical model's for the half-graben structures within the large keystone triangle could be complex, e.g., several grabens may form. We predict that a larger triangular keystone block occurs where an antithetic normal fault extends from the surface to the high-angle reverse fault at depths of -1.2 km. Analysis of uplift motion for longer times suggests the new secondary normal fault could form a graben, which initially moves downward to the left, but could become a high-angle reverse fault in its subsequent history.

EXPERIMENTAL ROCK DEFORMATION AND DRAPE FOLDS

Experimental folding of rocks under confining pressure generated drape folds in multi-layered specimens (Friedman et al., 1976). Deformation is characterized by generation of fault geometries, displacements, layer thickness changes and microfractures. When a linear saw cut is placed between blocks of brittle sandstone overlain by intact slabs of limestone, reverse faults curving concave downward propagate upward into passive ductile layers from the saw cut in the forcing block. With increasing displacement, successively younger reverse and normal faults occur in the upthrown block. Downthrown layers, thickened by uniform flow and fault repetition, are displaced away from the fault by bedding plane slip. Stress trajectories of σ_1 are inclined at low angles to layer boundaries near faults and become perpendicular to these boundaries away from the fault. Upthrown layers, extended parallel to layering and perpendicular to fold axes, show extension fractures, thinned layers, and development of graben zones and low-angle normal faults conjugate to the reverse faults. Stress trajectories of the reverse fault model are shown in Figure 13.

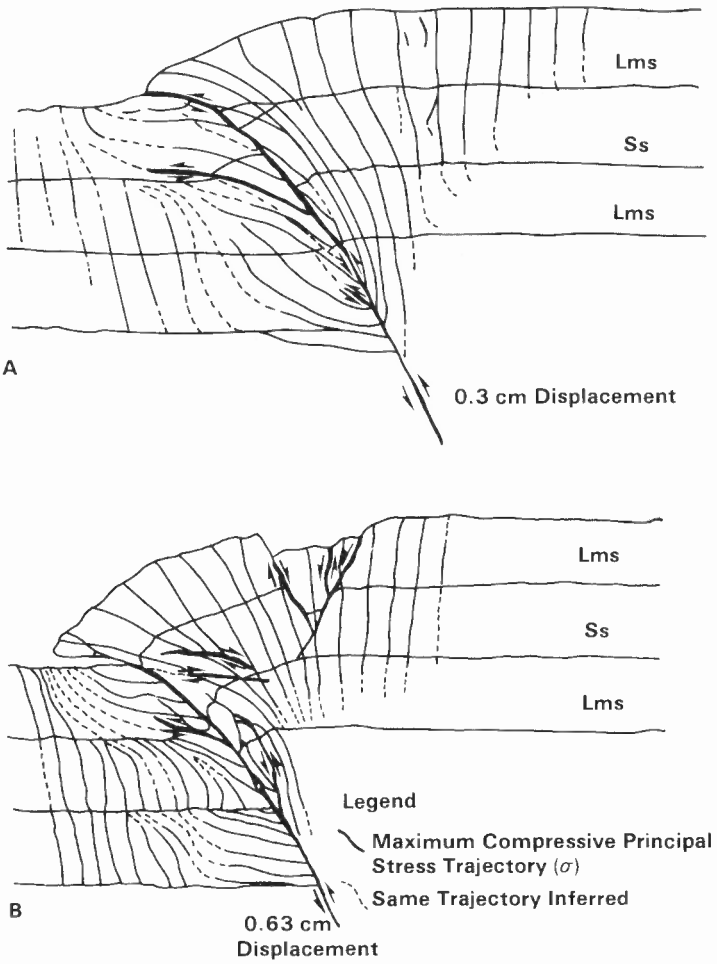


FIGURE 13. Experimental drape folds showing two stages of deformation and stress trajectories from micro-fracture orientations. The principal compressive stress orientations are essentially horizontal in the far field, but rotate in the near field as the fault zone is approached. In the hanging wall, these stresses are subparallel to the low-angle portion of the reverse fault. In the footwall, these stresses show a concave upward attitude below the reverse fault. Published with permission of John Logan, Center for Tectonophysics, Texas A&M University.

COMPARISON OF NUMERICAL AND EXPERIMENTAL MODELS

It is interesting to compare stress trajectories predicted by the numerical models and experimental fracture orientations. Numerical models assume an initial homogeneous layer of uniform thickness. The experimental models assume uniform thickness of several limestone and a sandstone layer. The numerical model calculates the principal stress orientations and provides an angle which is plotted relative to the x axis to determine stress trajectories. The relations of microfractures and calcite twin lamellae are used to generate stress trajectories in the experimental model.

In both models, principal compressive stress trajectories are normal to layer boundaries at some distance from the region influenced either by the reverse fault model, the graben model, or the layered experimental model. As mentioned in the section on deformation and stress analysis, the engineering orientations for σ_3 and geologic orientations for σ_1 are the same. As fault zones are approached, early deformation stages indicate that the hanging wall has a stress trajectory which becomes subparallel to the reverse fault. The footwall has a stress trajectory which is subparallel to the layer in the lower segment, but rolls up to become normal to the layer near the center of the concave reverse fault. In early stage of the experimental drape fold model, where motion on the saw cut was 0.3 cm, these stress trajectories present a smooth curve. In later stages, bedding plane slip allowed offset and stress trajectories, while still showing the general trends, are divergent. In the numerical model, no slip occurs between beds and stress trajectories curve upward from subparallel to the base to a horizontal orientation where the reverse fault begins to have a shallow dip and then back towards the shallow dipping thrust portion of the reverse fault. The numerical and experimental models show good overall correlation in orientations of stress trajectories in the hanging wall and the lower portion of the footwall during early stages of deformation, although divergence occurs in the upper portion of the footwall.

The initial numerical reverse fault model predicts occurrence of tensile stresses and shear failure zones near the surface where layer parallel extension occurs. Eventually two faults are predicted. When one fault is added, stress relief occurs in the immediate vicinity of the fault, but subsequent deformation predicts a second fault will be generated behind the first conjugate normal fault. In experimental models, normal faults occur at 0.063 cm of displacement above the sharp angle formed by

the saw cut and initial basal sandstone bedding. One dips subparallel to the reverse fault system below and the other is conjugate to the reverse fault.

Similarities between stress trajectories of numerical and experimental models indicate certain aspects of reverse faulting are becoming better understood. The occurrence of conjugate normal faults, which create graben structures in the experimental models, and triangular portions of the *keystone structures* of the numerical models are consistent. Occurrence of successively younger reverse faults or splays in the experimental model is consistent with numerous surface faults in structural cross sections of Baltz (1972). Drape folds and small graben features on the upthrown portions of basement blocks are part of the structural relations found throughout much of the Wyoming province (Berg, 1962; Wise, 1963; Prucha et al., 1965; Baltz, 1972).

KEYSTONE STRUCTURES

The process of evaluating dynamic stress fields and failure conditions during a faulting sequence provides intriguing scenarios for the genesis of reverse faulting. The cause of a single high-angle reverse fault is considered first. When a reverse fault occurs in a finite element model and the hanging wall is uplifted, upper regions above the low-angle portion of the reverse fault act like a triangular cantilever being pulled downward under the weight of body forces. A concave upward shape occurs in stress contours in the fault zone as stress decreases due to unloading. Since the footwall has also been unloaded during this process, the contour shape is asymmetrical for the stress field. As stress decreases in the hanging wall, failure is predicated by the finite element model and the loci of an antithetic normal fault occurs between the reverse fault and the surface.

Now consider the case where two faults, an antithetic fault and a high-angle reverse fault, occur. As the antithetic fault moves in conjunction with the hanging wall above the high-angle reverse fault, the stress field becomes more discontinuous. Three geologic structures, an uplifted hanging wall, a triangular region between the faults from the surface downward to a common vertex and a footwall undergo deformation. Naming this combination of distinct physical features a *keystone structure,* we evaluate the mechanical behavior. During the early phase of uplift of the hanging wall, the butt of the triangle undergoes extensile stress and a secondary normal fault is formed conjugate to the initial antithetic fault. With further uplift, the triangle undergoes a zone of compression whereas the surface of the hanging wall aft the antithetic fault remain extensile. In the final stage of uplift, the triangle's toe undergoes imbricate thrusting. A second, antithetic normal fault develops in the hanging wall aft the first. Dominant motion on the butt of the triangle is dip slip on the antithetic normal and thrusting in the toe on the hanging wall portion above the low-angle reverse fault. Thrusting is 5 times dip-slip motion.

The combined deformation process of the hanging wall, with its antithetic faulting, the triangular region which undergoes conjugate normal faulting and imbricate thrusting, and the unloading of the footwall defines a *keystone structure*. The stress state for the final uplift of the keystone structural model shown in Figure 14.

REVISED GEOLOGIC MODEL

Integrating geologic interpretations, where imbricate thrust faults were interpreted to show concave downward arcs to depth (Wise, 1963; Prucha et al., 1965; Baltz, 1972), and numerical analyses, where high-angle reverse faults were shown to have both normal and thrust types of displacements, we can predict other effects in the structural history of basement block faults, reverse faulting and uplift.

Surface geologic mapping provides real fault attitudes for only as much horizontal exposure as occurs in the region. Extrapolations beyond this point are based on interpretations which usually embody assumptions of a structural deformation style of that period of thought. For example, if faults are concave upward, horizontal compression was considered to create the process. Alternatively, if faults are concave downward, horizontal uplift was considered as the creative origin. Neither of these approaches was commonly based on congruent interpretation of geologic structures and numerical models to aid in interpretation.

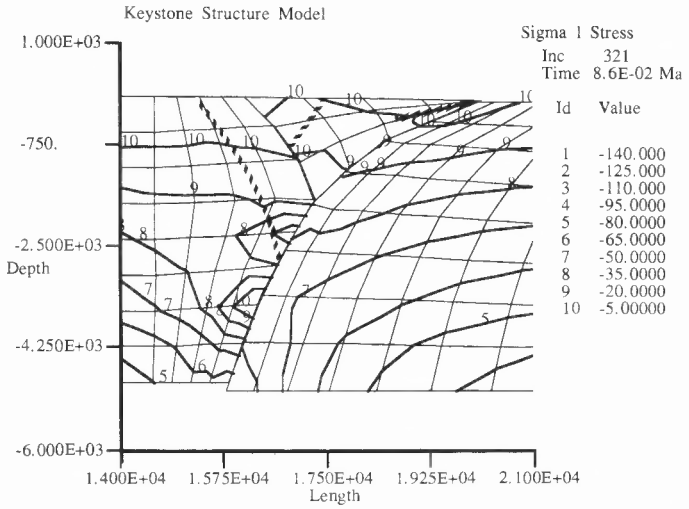


FIGURE 14. Stress magnitudes at the final stage of uplift in the keystone model. Additional faults are predicted at the butt of the triangle (conjugate normal shown by hachured line), toe (imbricate thrust shown by jagged line) and a second antithetic normal fault (shown by hachured line) is predicted in the hanging wall beneath the first. Tensile stress occurs in the hanging wall, extending to depths $\geq$0.5 km.

When the southeastern Sangre de Cristo structure of Baltz (1972) is analyzed in light of other field, experimental and numerical evidence, this model suggests a horizontal uplift origin through interpretation of the orientations of extrapolated faults. If extended to common depths of the numerical models, it is still both internally consistent and is congruent with analytical and numerical models. In effect, both geologic and numerical analyses indicate a high-angle reverse fault (or series of faults) can explain the occurrence of imbricate thrusts in the sedimentary layer and high-angle normal faults in the more uplifted portions of the structure through the *keystone structure concept* (as described in the section on keystone structure). Localized scales of surface data may only provide indirect or partial information on the occurrence of a *keystone structure*. The revised geologic models are shown in Figure 15.

DISCUSSION

The eastern flank of the southern Sangre de Cristo Mountains north of Las Vegas, New Mexico consists of several similar structural elements. Precambrian granitic highlands, a series of westward-dipping asymmetric monoclinal or drape fold structures of Paleozoic rocks cored by reverse or thrust faults, and a sequence of Paleozoic rocks covered by Mesozoic clastics in the lower Raton basin have been described by Baltz and Bachman (1956), Prucha et al. (1965) and Baltz (1972). Geologic structure sections in northern San Miguel County indicate three major fault-cored fold sequences occur at El Cielo Mountain, south of Hermit's Peak, and west of the Creston (Baltz and Bachman, 1956, section B-B′; Baltz, 1972, section B-B′). Prior analyses in essentially the same structural area provided surficial geologic structures with thrust and high-angle reverse faults as well as interpretations of both shallowing and steepening of faults with depth (Baltz and Bachman, 1956; Baltz, 1972). These faults were extrapolated to depths of 2–4 km.

Analytic and numerical models of the dynamic faulting process evaluated in this report provide the faulting history of reverse faults and more complicated geologic structures such as *keystone structures*. An elastic solution predicted the loci of a high-angle reverse fault on a 5 km deep structure of the basement above a step function in the basement which caused horizontal uplift (Sanford, 1959). Numerical solutions (scaled to the same dimensions and provided herein) include this loci as a discrete reverse fault, impose a single step function, and predict

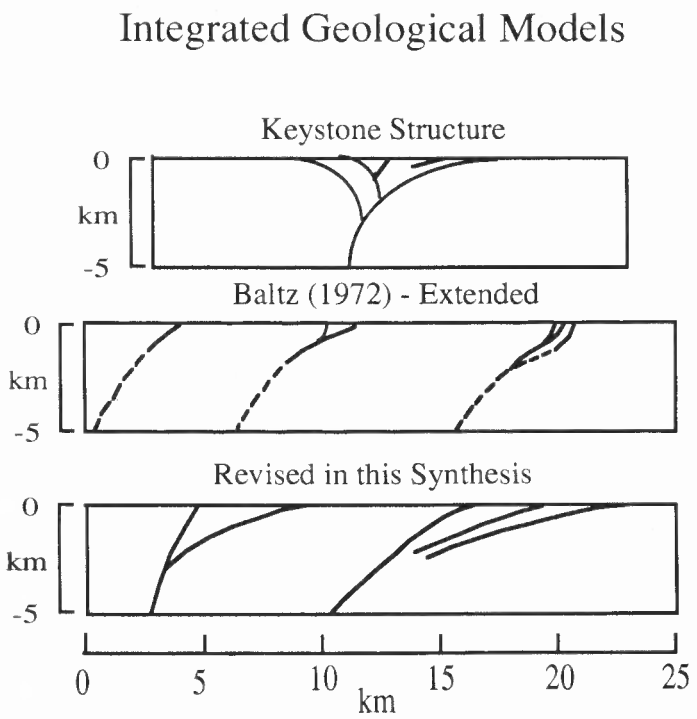


FIGURE 15. Comparison of keystone structural model with geologic interpretations of Baltz and Bachman (1956) and Baltz (1972). If one assumes the reverse fault model and progresses through its deformation to the keystone structure, the geologic data of Prucha et al. (1965) and the Baltz (1972) interpretations are interpreted in a new light. One reverse fault in the numerical model becomes three structural faults in the geologic case. A common reverse fault origin caused by horizontal uplift is suggested for structures of the southern Sangre de Cristo Mountains of northern New Mexico.

a second antithetic normal fault which defines a triangular structure in the hanging wall of the reverse fault.

When this second fault is placed in the structure, further calculations predict normal faults in the butt of the triangle conjugate to the antithetic fault, imbricate thrust faults in the toe of the triangle, and a subsequent antithetic normal fault aft the original in the hanging wall. The sequence of uplifted hanging wall structures, the triangle with intermediate uplift containing conjugate normal at the butt and imbricate thrust faults at the toe, and the relatively down-dropped footwall below the low-angle portion of the reverse fault are defined as a keystone structure.

Geologic structures of the southeastern flank of the Sangre de Cristo Mountains are interpreted by Prucha et al. (1965) and Baltz (1972) to consist of basement block uplifts where sediments are draped over reverse faults. These drape folds contain high-angle reverse and imbricate thrust faults in the sedimentary cover and steepen with depth in the basement. When structures are extended to 5 km of depth and compared with the keystone structure, strong similarities become evident. If only one series of imbricate structures is considered, the occurrence of imbricate thrusts predicted in the triangular toe of the numerical model overlying the low-angle portion of the reverse fault is consistent with the thrust and reverse faults in the geologic structures. When three similar structures occur, as Prucha et al. (1965) and Baltz (1972) have shown, then three reverse faults are required to explain this response. This suggests that assumptions of a simple step function causing horizontal uplift must be expanded to at least three (or more) steps in the basement uplift process.

If the triangular portion were all the numerical model to be considered, we would be done. Unfortunately, this limited analysis ignores antithetic normal and conjugate normal faults of the triangular portion of the keystone structure and the uplifted hanging wall! The region from the butt of the triangle to the toe in the keystone structure is uplifted and becomes compressed. When these structures are considered, the western unmapped portions or the Sangre de Cristo's come into play. Could this represent the region between Mt. Baldy east of Santa Fe and Elk Mountain just outside the western edge of sections from Prucha et al. (1965) and Baltz (1972)?

We must also consider implications of the antithetic and conjugate normal faults from the numerical model which form the butt of the triangle! These faults form prior to continued uplift of the hanging wall and triangular region. The eastern fault dips 60°, whereas the western fault initially has a shallower dip of 40°, but steepens with depth to 75°. Recent studies of surface structures in the southern Rocky and Sangre de Cristo Mountains (Prucha et al., 1965; Baltz, 1972; Grose, 1972; Tweto, 1975) contain basement-cored uplifts. A zone of west-dipping high-angle reverse faults and positive gravity anomalies (Cordell and Keller, 1984) is associated with the western flanks of the Sangre de Cristo Mountains. Prucha et al. (1965) pointed out the need to think at various levels of the physical process and unravel the surface data based on both the level of observation at the erosion surface and include mechanical and analytic conclusions. We add additional constraints by asking for consistency with experimental and geophysical data, e.g., gravity information.

Experimental folding of brittle rocks under confining pressure generated drape folds in overlying ductile rocks (Friedman et al., 1976). Upthrown layers, extended parallel to layering and perpendicular to fold axes, show extension fractures, thinned layers, and develop graben zones and low-angle normal faults conjugate to reverse faults. Downthrown layers, thickened by uniform flow and fault repetition, are displaced away from the fault by bedding plane slip. Stress trajectories of σ_1 are inclined at low angles to layer boundaries near reverse faults and become perpendicular to these boundaries away from the fault.

Similarities between stress trajectories of numerical and experimental models also indicate aspects of reverse faulting are becoming well understood. Occurrences of conjugate normal and antithetic reverse faults associated with the uplift described above, which create structures interpreted as graben structures in experimental models, and triangular portions of the *keystone structures* of the numerical models are consistent. Occurrence of successively younger reverse faults or splays in the experimental model is consistent with numerous imbricate surface faults in structural cross sections of Baltz (1972). Drape folds and small graben features on the upthrown portions of basement blocks are part of the structural relations found throughout much of the Wyoming province (Berg, 1962; Wise, 1963; Prucha et al., 1965; Baltz, 1972).

Gravity interpretations for the Rio Grande rift (Sanford, 1968; Cordell, 1976, 1979; Keller et al., 1984) indicate both estimates of shapes, depth of bolson fill, and depth to effective basement in the San Luis, Española and Albuquerque basins. Keller et al. (1984) indicate that north of Alamosa and near Taos, fill exceeds 3 km whereas near Española fill is about 2+ km. The compacted sedimentary rocks between basement and fill are estimated to be 2.5, 2.5 and 1 km respectively. Relative uplift is 8 km between basin deeps and adjacent mountain highs. The San Luis–Taos basin and Albuquerque basin are typically bounded by steep gravity gradients which shallow westward. The Española basin gravity gradients are more uniform, except for the influence of the Jemez Mountains and Velarde graben. Cordell (1976) attempted to relate gradients to faulting in the Rio Grande rift.

These basin fill gravity features with 5 km of bolson fill, Mesozoic (?) and Paleozoic sediments are consistent with a rift feature at the butt of the triangle for the keystone structure. A rift feature consists of asymmetric normal faults interacting at depth; an antithetic fault whose dip ranges from 40–75° and a conjugate normal fault dipping 60°.

IMPLIED SANGRE DE CRISTO STRUCTURES

Consider the following structural components to provide an integrated picture of the structural history of the southeastern flank of the Sangre de Cristo Mountains. From surface geology, several imbricate thrust or reverse fault zones core folds in sediments. Faults are interpreted to steepen with depth in underlying granites. From numerical experiments on dynamic deformation of reverse faults undergoing a simple horizontal step function, a keystone structure occurs. A keystone structure is one

where the hanging wall is uplifted and subsequent antithetic faults form a triangle as the tip of the hanging wall acts like a "cantilever" and fails under its own weight. The hanging wall and triangle undergo larger and smaller upward motions relative to the footwall, with additional normal faulting in the butt and imbricate thrust faulting at the toe of the triangle. The footwall is relatively downthrown. The region between the conjugate normal fault and imbricate thrust zone is a horst in the numerical model. The region between the antithetic and conjugate normal faults may become a rift graben. From experimental drape folding, the reverse fault splays, generating successively younger, concave downward reverse faults as uplift continues. In later stages of experimental deformation, uplift creases extensional features at the surface whereas downthrown sedimentary rocks thicken through flow and faulting.

When interdisciplinry efforts are integrated, the behavior of the southern Sangre de Cristo Mountains can be interpreted in a new light. Figure 16 is a model which integrates numerical, experimental and field geologic data to provide structural sections which contain the tilted fault blocks and associated drape folds with other regions of the Sangre de Cristo Mountains. The basement block features of Prucha et al. (1965) and Blatz (1972) are a series of basement blocks which are being uplifted along one or more reverse faults. Sediments are draped over tilted basement blocks. Faults coring asymmetric monoclines or drape folds are low-angle portions of reverse faults. The imbricate thrust faults are a function of compression in the toe of the triangular portion of the keystone structure. These structural sections become only part of an integrated model near the toe of a triangular region with one fault or a region where several reverse faults and imbricate thrust zones occur.

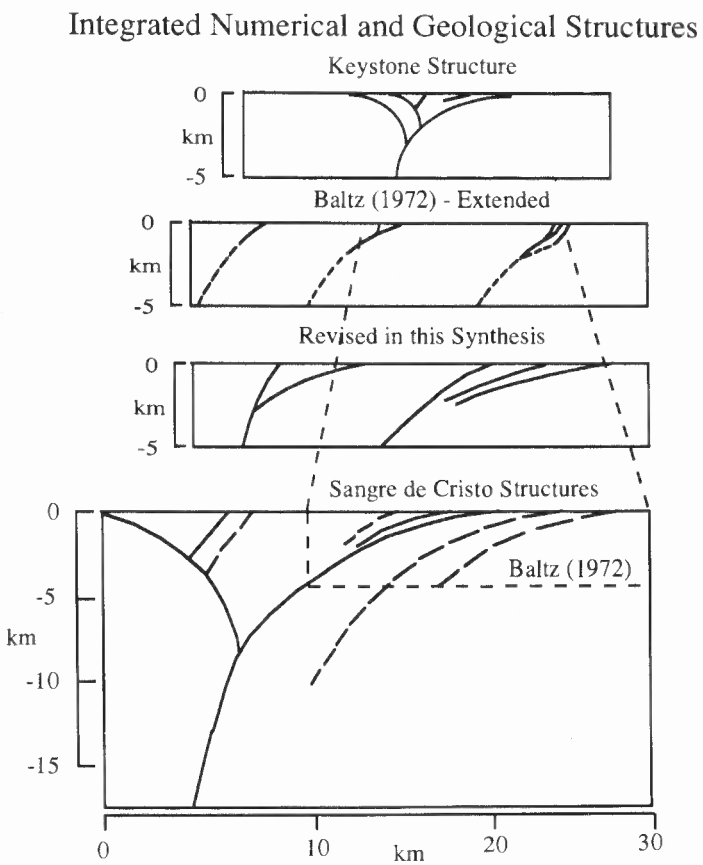


FIGURE 16. Integrated numerical and geological structures to the Sangre de Cristo Mountains of northern New Mexico. The principal change suggests that the series of three structures from Elk Mountain through El Cielo Mountain and into the lower Raton basin are reverse fault structures on the eastern side of the Sangre de Cristo Mountains. Evaluation of Figures 9 and 10 suggests a series of faults could be found in the highlands of the Sangre de Cristo Mountains, a region essentially unmapped.

The interior of the Sangre de Cristo's is a faulted highland to the north (Clark, 1966) which may represent the uplifted portion of the keystone structure model where compression dominates in early stages of uplift.

If more than one reverse fault exists, the splaying affect shown by experimental models could occur. Structural sections of Prucha et al. (1965) and Baltz (1972) represent only a portion of regional uplift. These rocks and their interpretative structural sections may either be only the low-angle portion of reverse faulting or be a series of reverse faults. Occurrence of several distinct regions of complex folds and reverse faults from the analysis of southeastern Sangre de Cristo Mountains suggests initial assumptions of Sanford (1959), experimental drape folding (Friedman et al., 1976), and this report for the shape of the process causing horizontal uplift may be too simplistic. One step function numerically produced a reverse fault and generated a keystone structure. In effect, this combined structure would account for one of Baltz's (1972) structural elements. The Sangre de Cristos would be the loci of a series of imbricate thrust and low-angle portions of reverse faults. To achieve several structural elements, the numerical model would need a series of basal step functions and reverse faults and would generate several attendant *keystone structures* or portions thereof. If other aspects of the keystone model are considered, then analyses must be made of the surface structures and the keystone structural concept.

IMPLIED RIO GRANDE RIFT AND SANGRE DE CRISTO STRUCTURES

The Sangre de Cristo Mountains, comprised of block uplifts and draped sediments on the eastern flank and faulted highlands in the interior, are bordered on the west by relatively down-dropped, faulted younger Tertiary features of the Rio Grande rift. Rift structural features consist of normal faults bounding grabens. Typically the east flank of the graben is the uplifted shoulder of the Sangre de Cristo Mountains. Near Taos, Clark (1966) provides structural interpretations of several inter-montane horst and graben structures consisting of the Taos Range, the Moreno Valley, and the Cimarron Range. Could these inter-montane features result from continued uplift to present elevations? Although the keystone structural model and the experimental mode only undergoes small amounts of uplift, natural structures generally have considerably greater uplift. This process may amplify faulting and cataclasis of basement block features until features near the surface of the uplifting triangle of the keystone structure are highly complex or have been removed by erosion. Wise (1963) indicates subsequent gravity sliding obscured some of the features of the Owl Creek Mountains.

What happens if we expand our scale for the keystone structure? Remember, the keystone structure consists of an uplifted faulted hanging wall, a set of both reverse and antithetic normal faults bounding a triangular shaped region, and a lower footwall. Another element of the keystone structure is found in the upper region of the butt of the keystone. After genesis of the antithetic normal fault which separates the cantilevered hanging wall and forms a keystone structure, conjugate normal faults occur to down-drop the smaller butt of the triangular keystone into a graben structure. In the deformed geometry, the surface of the hanging wall, the keystone and the footwall show gradations from higher to lower relief.

Gravity interpretations for the Rio Grande rift (Sanford, 1968; Cordell, 1976, 1979; Keller et al., 1984) indicate both estimates of shapes, depth of bolson fill and depth to effective basement in the San Luis, Española and Albuquerque basins. Rift-basin-fill gravity features with 5 km of bolson fill, Mesozoic (?) and Paleozoic sediments are consistent with generation of a rift feature at the butt of the triangle for the keystone structure. Asymmetric normal faults interact at depth in the numerical model; an antithetic fault whose dip ranges from 40–75° and a conjugate normal fault dipping 60° intersect. Does the presence of deep structural grabens bordering the Sangre de Cristo Mountains from Salida, Colorado, to Taos, New Mexico, as well as similar structures in the Albuquerque basin infer a series of normal faults bounding the Rio Grande rift and uplifted hghlands of the Sangre de Cristo's being the triangular portion of the keystone structure?

Can the eastern Sangre de Cristos, comprising imbricate thrusts of

the toe, be only one part of a triangular keystone or several low-angle reverse faults and the attendant footwall be the surface expression of a low-angle portion of one or more reverse faults? Could the keystone's butt, containing normal faults, explain combined origins of normal faults of the rift, uplift of intramontane grabens and horsts of the Sangre de Cristos', and imbricate thrusts and reverse faults associated with block faulting and basement uplift bordering the Raton basin? Viewed in this light, the western triangular portion of the keystone could form deep, sediment-filled rift features such as graben basins (San Luis, Española, Albuquerque) of the Rio Grande rift. The central portion of the triangular keystone could form complex highlands containing horsts and grabens near Taos and Cowles. The eastern portion of the footwall of the keystone structure could form imbricate thrusts associated with block faulting and basement deformation above crustal reverse faults for smaller ranges bordering the lower Raton basin. Figure 17 is a synthesis of regional structure from the Rio Grande rift through the relatively unmapped Sangre de Cristo Mountains to the uplifted tilted basement fault blocks of the southeastern Sangre de Cristo Mountains.

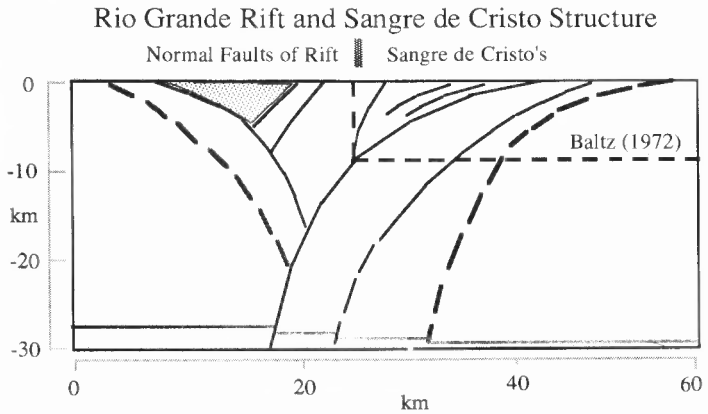


FIGURE 17. Rio Grande rift and Sangre de Cristo structure, Sangre de Cristo Mountains, northern New Mexico. Although certain features of the eastern side of the Sangre de Cristo Mountains can be explained by a portion of Figure 14, the keystone structure, with its conjugate normal faults in the triangular keystone and the antithetic fault which underlies it, must also be consistent. The conjugate normal faults are consistent with normal faults bounding the east side of the Rio Grande rift. Normal faults on the west side of the rift are consistent with antithetic faults conjugate to a series of underlying reverse faults.

ACKNOWLEDGMENTS

I thank W. R. Haneberg (New Mexico Institute of Mining and Technology) for his careful review of the original manuscript.

REFERENCES

Anderson, C. A., 1986, SANGRE: a finite element code for fluid migration, heat transport, and faulting in highly deformable, porous geologic media: LA-10666-MS, Los Alamos National Laboratory.

Baltz, E. and Bachman, R., 1956, Notes on the geology of the southeastern Sangre de Cristo Mountains, New Mexico: New Mexico Geological Society, Guidebook 7, pp. 96–108.

Baltz, E., 1972, Geologic map and cross sections of the Gallinas Creek area, Sangre de Cristo Mountains, San Miguel County, New Mexico: U.S. Geological Survey, Miscellaneous Geological Investigation Map I-673.

Baltz, E., 1978, Resume of Rio Grande depression in north-central New Mexico: New Mexico Bureau of Mines and Mineral Resources, Circular 163, pp. 210–227.

Berg, R. R., 1962, Mountain flank thrusting in Rocky Mountain foreland, Wyoming and Colorado: American Association of Petroleum Geologists Bulletin, v. 46, pp. 2109–2032.

Bridwell, R. J., 1990, Finding fault: Civil Engineering Magazine, Special Supplement, Engineering Solutions on Macintosh, June, 1990, in press.

Clark, K., 1966, Geology of the Sangre de Cristo Mountains and adjacent areas, between Taos and Raton, New Mexico: New Mexico Geological Society, Guidebook 17, pp. 57–65.

Cordell, L. E., 1976, Aeromagnetic and gravity studies of the Rio Grande graben in New Mexico between Belen and Pilar: New Mexico Geological Society, Special Publication, 6, pp. 62–70.

Cordell, L. E., 1979, Gravimetric expression of graben faulting in Santa Fe County and Española basin, New Mexico: New Mexico Geological Society, Guidebook 30, pp. 59–64.

Friedman, M., Handin, J., Logan, J. M., Min, K. D. and Stearns, D. W., 1976, Experimental folding of rocks under confining pressure; part III. Faulted drape folds in multi-lithologic layered specimens: Geological Society of America Bulletin, v. 87, pp. 1049–1066.

Grose, L. T., 1972, Tectonics; *in* Mallory, W. W., ed., Geologic atlas of the Rocky Mountains region: Denver, Rocky Mountain Association of Geologists, pp. 34–44.

Handin, J., Hager, R. V., Jr., Friedman, M. and Feather, J. N., 1963, Experimental deformation of sedimentary rocks under confining pressure; pore pressure tests: American Association of Petroleum Geologists Bulletin, v. 47, pp. 718–755.

Jaeger, J. C. and Cook, N. G. W., 1979, Fundamentals of rock mechanics (3rd edition). Chapman Hill Science Paperback, 593 pp.

Johnson, A. M. and Honea, E., 1975, A theory of concentric, kind, and sinusoidal folding and of monoclinal flexuring of compressible, elastic multilayers III, transition from sinusoidal to concentric-like chevron folds: Tectonophysics, v. 27, pp. 1–38.

Keller, G. R., Cordell, L., Davis, G. H., Peeples, W. J. and White, G., 1984, A geophysical study of the San Luis basin: New Mexico Geological Society, Guidebook 35, pp. 51–57.

Kelly, S. A. and Duncan, I. J., 1984, Tectonic history of the northern Rio Grande rift derived from apatite fission-track geochronology: New Mexico Geological Society, Guidebook 35, pp. 67–74.

Prucha, J. J., Graham, J. A. and Nickelsen, R. P., 1965, Basement-controlled deformation in Wyoming province of Rocky Mountains foreland: American Association of Petroleum Geologists Bulletin, v. 49, pp. 966–992.

Reches, Z. and Johnson, A. M., 1978, Development of monoclines: part II. Theoretical analysis of monoclines: Geological Society America, Memoir 151, pp. 273–311.

Sanford, A. R., 1959, Analytical and experimental study of simple geologic structures: Geological Society of America Bulletin, v. 70, pp. 19–52.

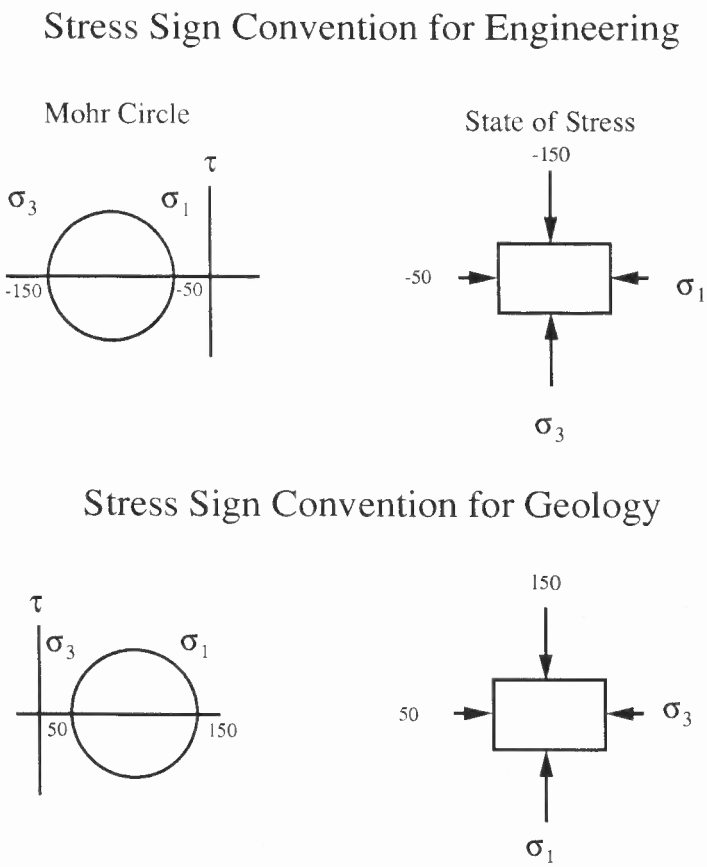


FIGURE 18. Comparison of state of stress for engineering and geologic sign conventions. Mohr circles and states of stress are shown for the same physical state.

Tweto, O., 1975, Laramide (Late Cretaceous–early Tertiary) orogeny in the southern Rocky Mountains: Geological Society of America, Memoir 144, pp. 1–44.

Wise, D., 1963, Keystone faulting and gravity sliding driven by basement uplift of Owl Creek Mountains, Wyoming: American Association of Petroleum Geologists Bulletin, v. 47, pp. 586–598.

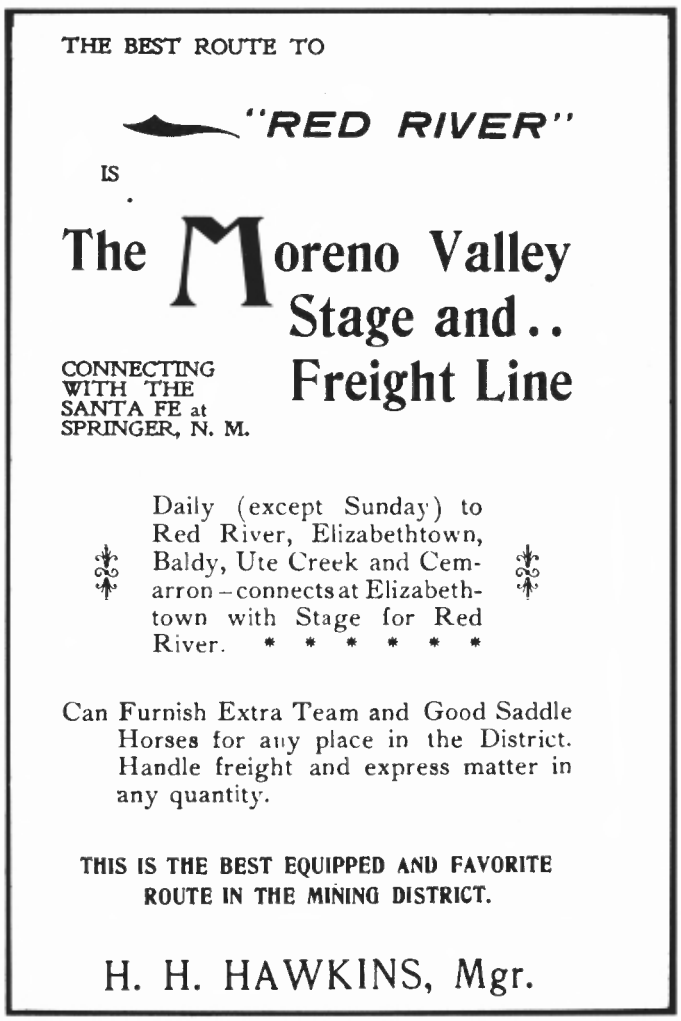
Woodward, L. A. and Ingersoll, R. V., 1979, Phanerozoic tectonic setting of Santa Fe County: New Mexico Geological Society, Guidebook 30, pp. 51–57.

APPENDIX—STRESS SIGN AND TERMINOLOGY CONVENTIONS

The only difference between engineering and geologic conventions is sign; the equations remain exactly the same, but have been multiplied by -1 (Jaeger and Cook, 1979). Consider the case where $\sigma_1 > \sigma_3$. Terminology for the engineering sign convention is as follows. The largest negative stress, e.g., -1000 MPa, is algebraically the minimum principal compressive stress or σ_3. The smallest negative stress, e.g., -100 MPa, is algebraically the maximum principal compressive stress or σ_1. The engineering term *minimum compressive principal stress, or* σ_3, represents the stress with the largest absolute value.

Geologically, compressive stress is positive and tensile stress is negative. Consider the case where $\sigma_1 > \sigma_3$. The maximum principal compressive stress would be 1000 MPa whereas the minimum principal compressive stress would be 100 MPa. These two stress conventions are shown diagrammatically in Figure 18.

A change in terminology is required to relate the two conventions. The minimum principal compressive stress for engineering σ_3 has the largest absolute value and is *equivalent* to the maximum principal compressive stress for geology σ_1.



The very phrase "stage coach" or "stage line" conjures up romantic images of beautiful Concords, pulled by matched sixes, gliding across mountains and prairies. Far from it; more often than not the "stage" was an open buckboard, or if one was particularly lucky, a canvas-covered hack or mud wagon which offered little protection from the road or elements. And the traveler paid dearly for the privilege, too—at the princely sum of $0.15 per mile, he was likely to part with a $10 gold piece (meals excluded) for his day's adventure. H. H. Hankin's [*sic*] Moreno Valley Stage Line was quite typical of turn-of-the-century accommodations. Leaving Springer soon after the arrival of the Santa Fe passenger train ("no later than 4:00 p.m."), the stage headed for Cimarron 24 miles distant, and arrived at the "popular Hotel Hankin" in time for supper (i.e., before 9:00 p.m.). Completely refreshed, the traveler could continue on his way to E'town or Red River the following morning—and part with another $10 gold piece in the process. Although fondly remembered, stagecoaching died quickly upon the arrival of the railroads. From Red River Gold Fields pamphlet, courtesy of University of Colorado.